Indian Journal of Chemistry
Vol. 64, April 2025, pp. 434-440
DOI: 10.56042/ijc.v64i4.17386

A comparative study of the catalytic activity of ZnO nanostructures prepared using microwave and sol-gel method: A green approach

Lekshmi S*, Aswathi H & Aiswarya L

Post Graduate Department of Physics and Research Centre, Sanatana Dharma College, Alappuzha 688 003, India
E-mail: lekshmisdc@gmail.com

Received 22 February 2025; accepted(revised) 24 March 2025

The present study reports the structural, optical and catalytic studies of green synthesised ZnO nanostructure using microwave and sol-gel method. The materials are characterised using XRD, FTIR, Raman and UV-Vis diffuse reflectance spectroscopic analysis. The XRD analysis reveals the formation of hexagonal wurtzite ZnO with an average crystalline size of 47.2 nm and 32.4 nm, respectively for ZnO prepared using microwave (Zno-M) and sol-gel method (ZnO-S). The catalytic activity of the nanostructures are analysed with the nitrophenol reduction in the presence of $NaBH_4$, indicating the superior performance of ZnO-M compared to ZnO-S. The optimised nanostructure exhibit a conversion efficiency of 97.3% with a first order rate constant of 0.44 min^{-1}. This study highlights the effectiveness of the synthesized ZnO nanostructures in detoxifying 4-nitrophenol from aqueous solutions.

Keywords: Green synthesis, Sol-gel, ZnO, Catalysis

Metal oxide nanoparticles have gained much attention in various fields such as catalysis[1], sensors[2], optoelectronics[3], photovoltaics[4], *etc.* In the recent years, metal oxide nanoparticles are considered as an efficient catalyst for the transformation of toxic nitroaromatic compounds into amines. The globalization and industrialisation have significantly increased with the use of different phenolic components. These are widely used in different industries such as textile, rubber fertilizers, paints *etc.*[5]. However, pollutants from these industries contribute to carcinogenic effects on the environment. Phenols in water typically form various derivatives, among which *para*-nitrophenol (PNP) is a toxic pollutant released from the industrial waste of dyes, pesticides, agrochemicals *etc.* On the other hand, nearly 27% of PNP is used in pesticide production such as parathion, while 13% is utilized in the synthesis of dye components. The maximum permissible concentration of nitrophenols in drinking water is 0.5 μmol L^{-1}. Due to its carcinogenic properties, PNP has been classified as a priority pollutant by the United States Environmental Protection Agency (USEPA)[6]. Therefore, the reduction of PNP to a non-toxic *Para*-Aminophenol (PAP) is essential before releasing to the environment. PAP is extensively utilized in the production of corrosion inhibitors, anti-corrosion lubricants, photographic developers, as well as in the manufacturing of antipyretic and analgesic drugs[7].

The catalytic reduction of PNP with zinc oxide as a catalyst gained attention due to its remarkable physiochemical properties. Rasaki *et al.* used a facile liquid precipitation citrate reduction process for the synthesis of Ag/ZnO nanorods with appreciable reduction capacity [8]. A hydrothermal co-precipitation route was used by Behera *et al.* for the synthesis of Maghemite/ZnOnanocomposite[9]. This composite shows excellent catalytic activity compared to pure oxide and it is found to be stable for five consecutive cycles. Recently a biogenic synthesis route was employed by Palanivel *et al.* for the synthesis of bare ZnO with an excellent catalytic property and stability[10].Nagaraja *et al.* synthesised ZnO using *Cordia myxa*gum for the effective use in the PNP reduction. The catalyst shows a complete reduction of 4-NP in the excess of $NaBH_4$within 15min, with recyclability and pseudo-first-order kinetics with a rate constant of 0.2571 min^{-1} (Ref. 11). Besides these, there are several works published on the catalytic activity of ZnO based composite materials such as CNT[12], MoS_2[13], and ZnO/CuO (Ref. 14). As the catalytic activity of the material depends on the synthesis method, here we used a simple cost effective green mediated synthesis of ZnO nanostructure using sol-gel and micro wave method. The catalytic application of this nanostructured material is then analysed by monitoring the reduction of PNP to NMP in excess $NaBH_4$.

Materials and methods

Materials

Zinc Nitrate hexahydrate (Zn $(NO_3)_2 \cdot 6H_2O$, 98%) was purchased from Merck. *Eupatorium odoratum* was collected from campus garden and taxonomically confirmed. Sodium borohydride ($NaBH_4$) was purchased from MedilisePvt. Ltd, India and *p*-nitrophenol (99%) from SRL Pvt. Ltd., India.

Extraction of leaf extract

1g of leaf was weighted and washed in tap water several times followed by a continuous wash in double distilled water. The washed leaves were boiled with 200 ml of double distilled water until the volume becomes 50 ml. The extract was then vacuum filtered using Whatman filter paper and stored in refrigerator for further studies.

Synthesis of ZnO using Microwave Method (ZnO-M)

1g of Zn $(NO_3)_2 \cdot 6H_2O$ was dissolved in 25 ml of leaf extract and stirred for 30 min at room temperature. The mixture was then subjected to microwave for 20 min and the obtained powder was then calcinated at 400°C for 2 hr to get ZnO nanostructure.

Synthesis of ZnO using sol-gel Method (ZnO-S)

1g of $Zn(NO_3)_2 \cdot 6H_2O$ was dissolved in 25 ml of leaf extract and stirred at a temperature of 150°C until the complete evaporation of solvent. The obtained powder was then calcinated at 400°C for 2 hrs to get ZnO nanostructure.

Characterisation

The XRD patterns of the samples were examined using a Bruker D8 advance X-ray powder diffractometer equipped with CuKα radiation (λ = 1.5406 Å). Diffuse reflectance spectra were recorded with UV-visible spectrometer (Shimadzu, UV-2600). Raman spectra are recorded using a 532 nm laser using a HORIBA XploraPlus Micro Raman spectrometer. Thermo-Scientific Nicolet iS50 instrument was used to record FTIR spectrum.

Catalytic studies

The catalytic activity of the materials is analysed using the efficiency of conversion of –nitrophenol to *p*-amino-phenol. For this, approximately 1 mg of catalyst was added to 3 ml of solution containing 3 mL of 0.1 mM *p*-nitrophenol. After that, 0.2 mL of $NaBH_4$ (0.2 M) was added to the solution. The catalytic activity was then evaluated using spectrometric approach using UV-visible spectra

Results and Discussion

XRD Analysis

The crystalline structure and crystalline size of the synthesised nanostructures were identified by XRD analysis. The XRD patterns of the ZnO prepared using microwave and sol-gel method is shown in Fig. 1. The XRD peaks at 2θ values of 31.8, 34.5, 36.23, 47.5, 56.6, 65.8, 66.4, 67.9, 69.1 and 77° corresponds to the reflection from (100), (002), (101), (102), (110), (103),(200(112) (201) and (202) crystalline planes of hexagonal WurtziteZnO (ICDD No. 01-007-2551). The sharp and well defined XRD peaks confirm the highly crystalline nature of the prepared sample. Moreover, no other impurity peaks are identified, validating the high purity of the prepared ZnO nanoparticles. The average crystalline size of the nanoparticles is calculated using Scherer equation (Equation 1)[15].

$$D = \frac{k\lambda}{\beta cos\theta} \quad ...(1)$$

where k is a constant (0.9), β is the full width at half maximum measured in radian and θ is the diffraction angle. According to the above equation, the average particle size was estimated to be 47.2 nm and 32.4 nm for ZnO-M and ZnO-S respectively.

The dislocation density (δ) of the sample was determined using the crystallite size as a basis. It is inversely proportional to the square of the crystallite size. Consequently, a higher dislocation density corresponds to greater hardness. Using the Equation 2[1], the dislocation density was calculated to be 4.5×10^{14} and $9.5\times10^{-14} m^{-2}$ respectively, for ZnO-M and ZnO-S.

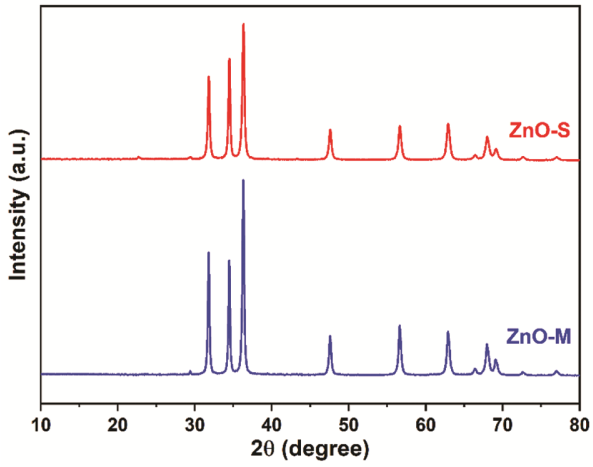

Fig. 1 — XRD pattern of ZnO prepared using microwave and sol-gel method

$$\delta = \frac{1}{D^2} \quad ...(2)$$

The micro-strain of the sample was estimated according to the Equation 3[15] and the value was found to be 8.9×10^{-4} and 8.34×10^{-4}, respectively for ZnO-M and ZnO-S. Therefore, it is inferred that the synthesis method significantly affects the structural properties of the nanostructures.

$$S = \frac{\beta cos\theta}{4} \quad ...(3)$$

Vibrational Spectroscopic Analysis

The formation of ZnO nanostructure was further confirmed by FTIR spectrum and is shown in Fig. 2. The strong band centred around 408 cm^{-1} in ZnO-M and 404 cm^{-1} in ZnO-S can be attributed to the Zn-O stretching vibration in the samples[16]. The band cantered at 874 cm^{-1} is attributed to –OH stretching vibration. A strong band was observed at 1410 and 1414 cm^{-1}, respectively in the samples ZnO-M and ZnO-S can be assigned to the OH bending vibrations of the absorbed water molecules on the surface of the samples[17].

The Raman spectra of the samples are shown in Fig. 3. ZnO is categorized under the C_{6v}^4($P6_3mc$) space group, exhibiting a hexagonal wurtzite arrangement. The Raman vibrational modes for ZnO nanostructures can be represented as follows[18,19].

$$\Gamma = 2A_1 + 2E_2 + 2E_1 + 2B_1 \quad ...(4)$$

The polar modes A_1 and E_1 can split into TO and LO modes with TO representing transverse vibrations and LO signifying longitudinal vibrations. In contrast, the E_2 mode is non-polar and is composed of two distinct frequencies, one low and the other high. The spectra of the prepared ZnO samples show significant vibrational peaks at 331, 381, 435, and 583 cm^{-1}. Particularly the strong peak at 435 cm^{-1}, which corresponds to the E_2 mode and displays the highest intensity. This distinct E_2 mode peak, observed at around 435 cm^{-1}, confirms the Wurtzite structure of the synthesized ZnO nanostructure. Additionally, a lower-frequency E_2 mode at 100 cm^{-1} is attributed to the vibration of the heavy Zn sub lattice. The Raman bands cantered at 381 and 583 cm^{-1} are associated with the A_1-TO modes and A_1-LO modes, respectively. Moreover, a band centered at 331 cm^{-1} is identified, which can be attributed to the second-order Raman scattering originating from the Zone boundary phonons ($2E_2$)[20]. Similar findings were previously reported by Rajalekshmi *et al.* [21].

UV-Vis Diffuse Reflectance Spectroscopic Studies

The optical characterisation of the prepared samples was analysed by recording the diffuse reflectance spectrum in a wide range of wavelength 1000 to 200 nm. The diffuse reflectance spectrum of ZnO-M and ZnO-S is shown in Fig. 4 (a) and (b), respectively, where a strong adsorption was observed from 500 nm. The optical band gaps of the materials are calculated using the Kubelka–Munk function (Equation 5)[21].

$$F(R) = \frac{(1-R)^2}{2R} \quad ...(5)$$

ZnO is classified as a semiconductor possessing a broad direct band gap. This band gap value can be determined through the graphical representation of $(F(R)h\nu)^2$ *versus* hν, wherein the x-intercept of this graph (Tauc plot, as illustrated in Fig. 4(c) and (d))

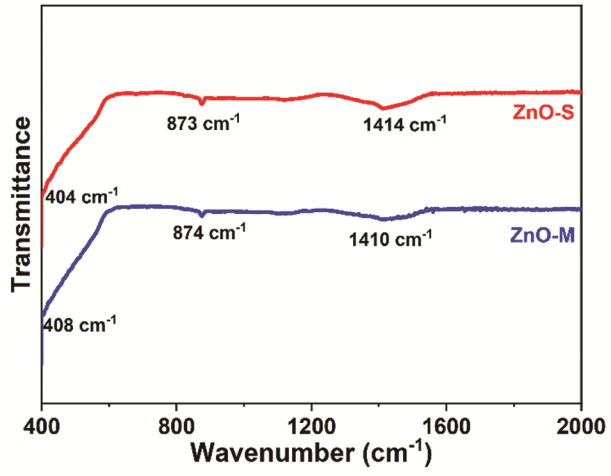

Fig. 2 — FTIR spectrum of ZnO-M and ZnO-S

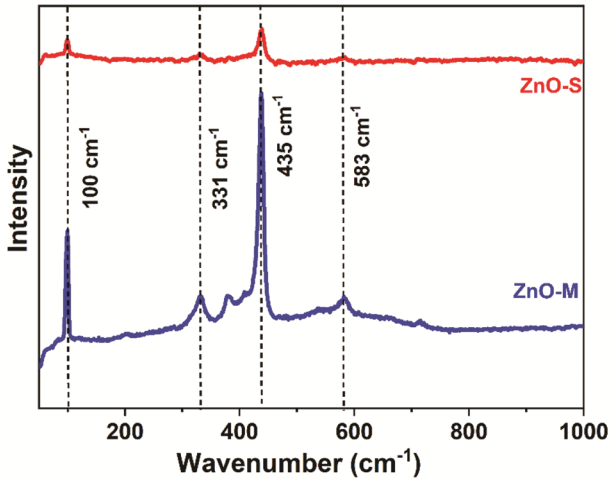

Fig. 3 — Raman spectrum of ZnO-M and ZnO-S

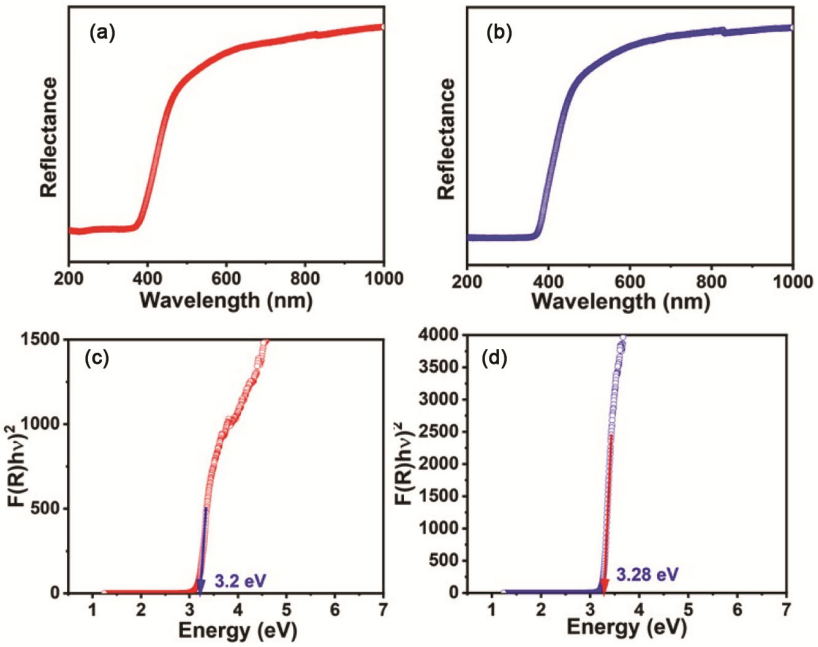

Fig. 4 — UV-Vis reflectance spectrum of (a) Zno-M , (b) ZnO-S, Taue plot of (c) ZnO-M and (d) ZnO-S

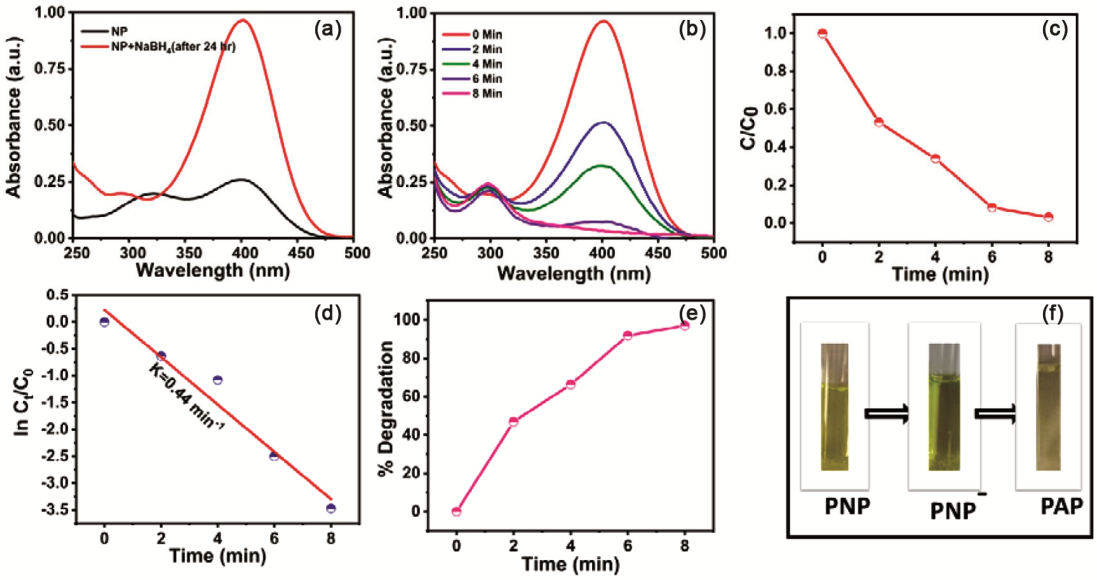

Fig. 5 — UV-Visible absorption spectra of catalytic reduction of PNP (a) without catalyst ZnO-M (b) with catalyst at different time intervals (c) Plot of C_t/C_0 with time (d) Plot of ln (C_t/C_0) v/s time (e) Percentage degradation of PNP at various time intervals (f) Colour change of PNP using reduction process.

provides the corresponding band gap value. The band gap energy of the prepared ZnO-S and ZnO-M is found to be 3.28 eV and 3.20 eV, respectively.

Catalytic Study

To evaluate the effectiveness of ZnO as a catalyst, the reduction of PNP was chosen as a benchmark reaction, facilitated by $NaBH_4$. A thorough analysis of the catalytic process was conducted using a UV-Visible absorption spectrophotometer. The initial absorption peak of the PNP aqueous solution was observed at 317 nm, and with the introduction of $NaBH_4$, it shifted to 400 nm, indicating the formation of phenolate ions. The intensification of the yellow colour further confirmed the presence of these phenolate ions. In Fig. 5(a), the UV-Visible spectrum illustrates the

reduction of PNP by $NaBH_4$ in the absence of ZnO-M nanocatalyst. From this graph, it's clear that even after 24 hours of reaction time, the peak intensity at 400 nm remains relatively unchanged. This underscores the need for a potent catalyst to accelerate the reaction rate, as the reduction of PNP is feasible from a thermodynamic perspective but hindered kinetically due to the repulsion between nitrophenolate ions (PNP-) and BH^{4-} ions. The introduction of a catalyst provides an ample surface area for PNP^{-} and BH^{4-} ions to adsorb, enabling a favourable reaction to take place. The inclusion of ZnO nanoparticles into the reaction mixture triggers a rapid reduction in the intensity of phenolate ions, leading to the emergence of a new peak at 300 nm, associated with the formation of *P*-Aminophenol. When ZnO nanoparticles are present, the reduction in peak intensity at 400 nm vividly signifies the progress of the reaction, which is nearly complete within 8 minutes, as depicted in Fig. 5(b). Simultaneously, there is a noticeable increase in intensity at 300 nm alongside the decrease in intensity at 400 nm[1].

Fig. 5(c) illustrates the evolution of the C_t/C_0 ratio over time. The decreasing trend in C_t/C_0 as time progresses indicates the advancing catalytic effectiveness of ZnO-M nanoparticles. This investigation also delved into the kinetics of the reduction process. In contrast to the PNP concentration (0.1 mM), the concentration of $NaBH_4$(0.2 M) is significantly higher. Consequently, the concentration of $NaBH_4$ remains consistent throughout the reduction sequence, establishing the reaction's reliance solely on the concentration of PNP. As a result, the reaction follows a pseudo-first-order kinetics pattern, and the utilization of Equation 6 allows for the determination of the associated rate constant[1].

$$ln\left(\frac{C_t}{C_0}\right) = -kt \qquad ...(6)$$

where, t is the time of reaction, k is the rate constant, C_0 and C_t are the concentration of PNP at the beginning and at time t, respectively. The plot depicted in Fig. 5(d) demonstrates the linear relationship between the natural logarithm ln (C_t/C_0) and time, indicating a consistent correlation. The calculated rate constant from this analysis is determined to be 0.44 min^{-1}, which provides validation for the pseudo-first-order nature of the reduction process. With the involvement of the CNp catalyst, a remarkable reduction of 97.3% in PNP is achieved, as calculated using the following Equation 7[22]:

$$Percentage\ of\ degradation = \frac{C_0 - C_t}{C_0} \times 100 \qquad ...(7)$$

Fig. 5(e) and Fig. 5(f) illustrate the calculated conversion efficiency of the ZnO-M nanocatalyst at intervals of 2 minutes and the change in colour in the PNP solution throughout the reduction process, respectively.

Similarly, in the Fig. 6(a), the UV-Visible spectrum illustrates the reduction of PNP by $NaBH_4$ in the

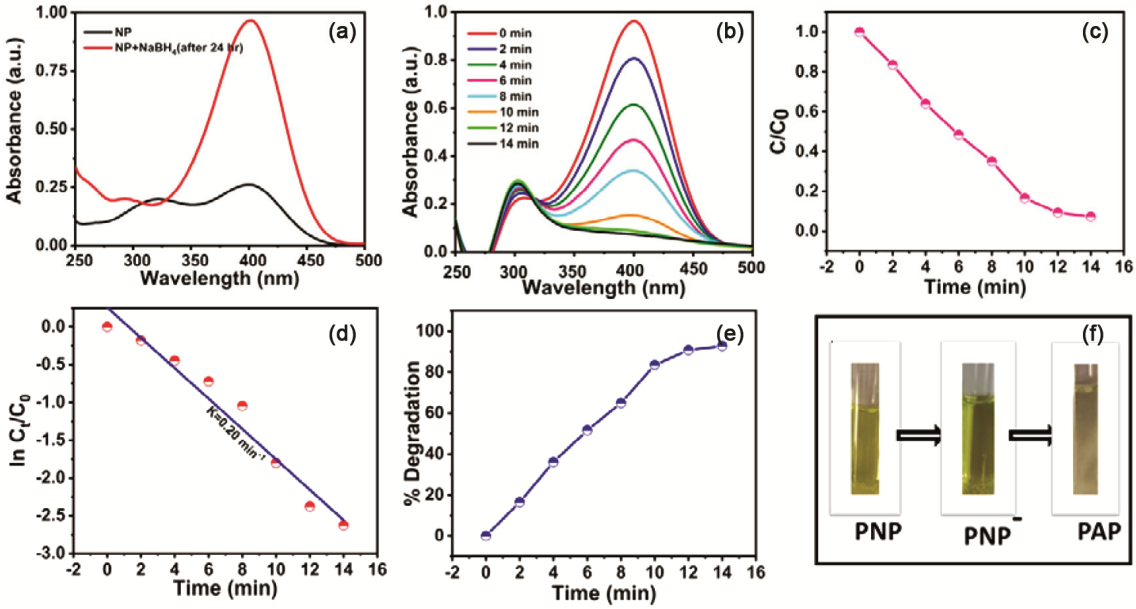

Fig. 6 — UV-Visible absorption spectra of catalytic reduction of PNP (a) without catalyst ZnO-S (b) with catalyst at different time intervals (c) Plot of C_t/C_0 with time (d) Plot of ln (C_t/C_0) v/s time (e) Percentage degradation of PNP at various time intervals (f) Colour change of PNP using reduction process

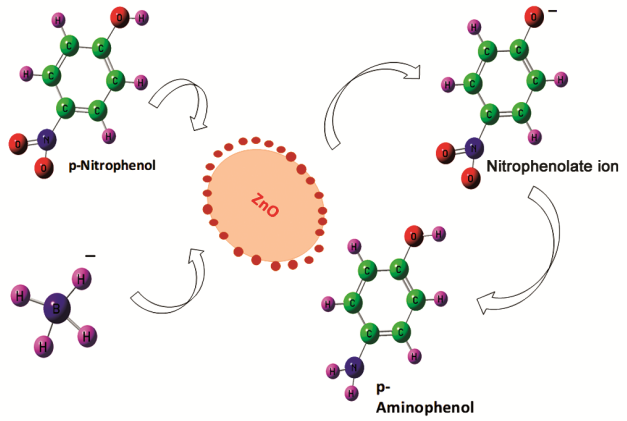

Fig. 7 — Schematic mechanism of reduction of PNP to PAP

absence of ZnO-S nanocatalyst. From this graph, it's clear that even after 24 hours of reaction time, the peak intensity at 400 nm remains relatively unchanged. In the presence of ZnO-S nanoparticles, the reduction in peak intensity at 400 nm vividly demonstrates the advancement of the reaction, which is nearly complete within 12 minutes, as depicted in Fig. 6(b). The effectiveness of the catalyst is evident from the C_t/C_0 *vs* time plot shown in Fig. 6(c). The catalytic activity of this reaction is also following first order kinetics. The calculated rate constant from this analysis is determined to be 0.20 min^{-1}, which provides validation for the pseudo-first-order nature of the reduction process (Fig. 6(d)). With the involvement of the CNp catalyst, a remarkable reduction of 96.5% in PNP is achieved (Fig. 6(e)). The change of colour of 4-Nitrophenol after 14 min of catalytic reaction is shown in Fig. 6(f).

The mechanism underlying the reduction of PNP is elucidated in Fig. 7. The central stage in the reduction of PNP involves the adsorption of BH^{4-} and PNP onto the surface of the nanocatalyst. In this sequence, BH^{4-} serves as an electron donor, while PNP acts as an electron acceptor. ZnO nanoparticles, functioning as a mediator, enhance the smooth transfer of electrons. The self-hydrolysis of $NaBH_4$ gives rise to the generation of BO^{2-} ions and the formation of active hydrogen species on the catalyst's surface. This active surface hydrogen, combined with electrons originating from BH^{4-}, are subsequently transferred to the $–NO_2$ group of PNP. This progression leads to the creation of an unstable intermediate named nitrosophenol, which swiftly transforms into a 4-hydroxyphenolate ion. Ultimately, the development of 4-aminophenol transpires, constituting the step that determines the rate of the overall reduction process[23]. The efficient transfer of electrons and the effective release of the resulting 4-aminophenol contribute to the catalytic effectiveness of ZnO.

Conclusion

ZnO nanostructure was synthesised using a facile green mediated microwave and sol-gel method. The structure, optical and morphological studies of the prepared material was studied using XRD, FTIR, RAMAN and UV visible diffuse reflectance spectroscopy. X-ray diffraction study revealed that the synthesized ZnO sample have hexagonal Wurtzite crystal structure irrespective of the synthesised method. Among the two ZnO, the material synthesised using microwave assisted method exhibited better catalytic activity with 97.3% of conversion efficiency. The better catalytic activity towards 4-nitrophenol reduction makes it as a perfect candidate for future environmental solution.

Acknowledgments

The authors acknowledge KSCSTE, Government of Kerala and the DST, Government of India for the instrumentation facilities provided under the FIST schemes (SR/FIST/College-227/2014(c).

References

1 Johnson E, Raji R K, Shine R C & Prema K H, *J Sol-Gel Sci Tech,* 107 (2023) 697.
2 Kaur M, Kailasaganapathi S, Ramgir N, Datta N, Kumar S, Debnath A K, Aswal D K, & Gupta S K, *App Surface Sci,* 394 (2017) 258.
3 Sreedharan R S, Krishnan R R, Bose R J, Kavitha V S, Suresh S, Vinodkumar R, Sudheer S K & Pillai V P M, *J Luminescence,* 184 (2017) 273.
4 Amador P-T, Mingorance A, Tanenbaum D & Mónica L-C, *The future of semiconductor oxides in next-generation solar cells*, (Elsevier), 2018, pp. 267.
5 Waseem R, Lee J, Raza N, Luo Y, Kim K-H & Yang J, *J Indus Eng Chem*, 71 (2019) 1.
6 Sasireka V, Roy A, Mariam E, Krishnamurthy S, Sundaram S & Mallick T K, *Scientific Rep*,13 (2023) 9521.
7 Sahu K, Singhal R & Mohapatra S, *Cat Lett,* 150 (2020) 471.
8 Abolaji R S, Zhao C, Wang R, Wang J, Jiang H & Yang M, *Mat Res Bull*, 119 (2019) 110536.
9 Meerambika B, Tiwari N, Basu A, Mishra S R, Banerjee S, Chakrabortty S & Tripathy S K, *Adv Powder Tech*, 32 (2021) 2905.
10 Palanivel D, Andal V, Ranganathan S, Cingaram R & Sundramurthy K N, *J Indian Chem Soc*, 101 (2024) 101337.
11 Nagaraja K & Hwan O T, *Int J Bio Macromol*, 253 (2023) 126788.
12 Alamro F S, Mostafa A M, Ahmed H A &Toghan A, *Surfaces Interfaces*, 26 (2021) 101406.
13 Madhushree R, Jadan R J U C, Dephan P &Sunaja D K R, *App Sur Sci Adv*, 10 (2022) 100265.

14 Feng A, Lin C, Zhou H, Jin W, Hu Y, Li D & Li Q, *Green Chem Eng*, 5 (2024) 205.
15 Manju V, Rohith R, Prasannakumar A T, Bhavija B V & Varma S J, *New J Chem*,46 (2022) 19874.
16 Worku A K, Delele W A, Nigus G H, Getu A M, Temesgen A Y, Negese Y M &Minbale A T, *SN App Sci*, 3 (2021) 1.
17 Kamboj M, Sharma P & Ram C, *Results Optics*, 10 (2023) 100371.
18 Batista-Grau P, Sánchez-Tovar R, Fernández-Domene R M & García-Antón J, *Surface Coatings Tech,*381 (2020) 125197
19 Pandey P, Mohammad R P, Fozia Z H &Kurchania R, *J Mat Sci Mat Elec*, 28 (2017) 1537.
20 Vinodkumar R, Navas I, Porsezian K, Ganesan V, Unnikrishnan N V & Pillai V P M, *Spectrochim Acta Part A Mol BiomolSpect*, 118 (2014) 724.
21 Rajalakshmi M, Arora A K, Bendre B S &Mahamuni S, *J App Phy,* 87 (2000) 2445.
22 Krishnan R R, Prasad E & Prema K H, *New J Chem*, 47 (2023) 4790.
23 Raji R K, Chandran S R, Jhonson E, Raveendrakurup R & Hariharan P K, *Chem Sel,* 7 (2022) e202201554.